Edinburgh
Student Journal of Science
Volume 1
Issue 3

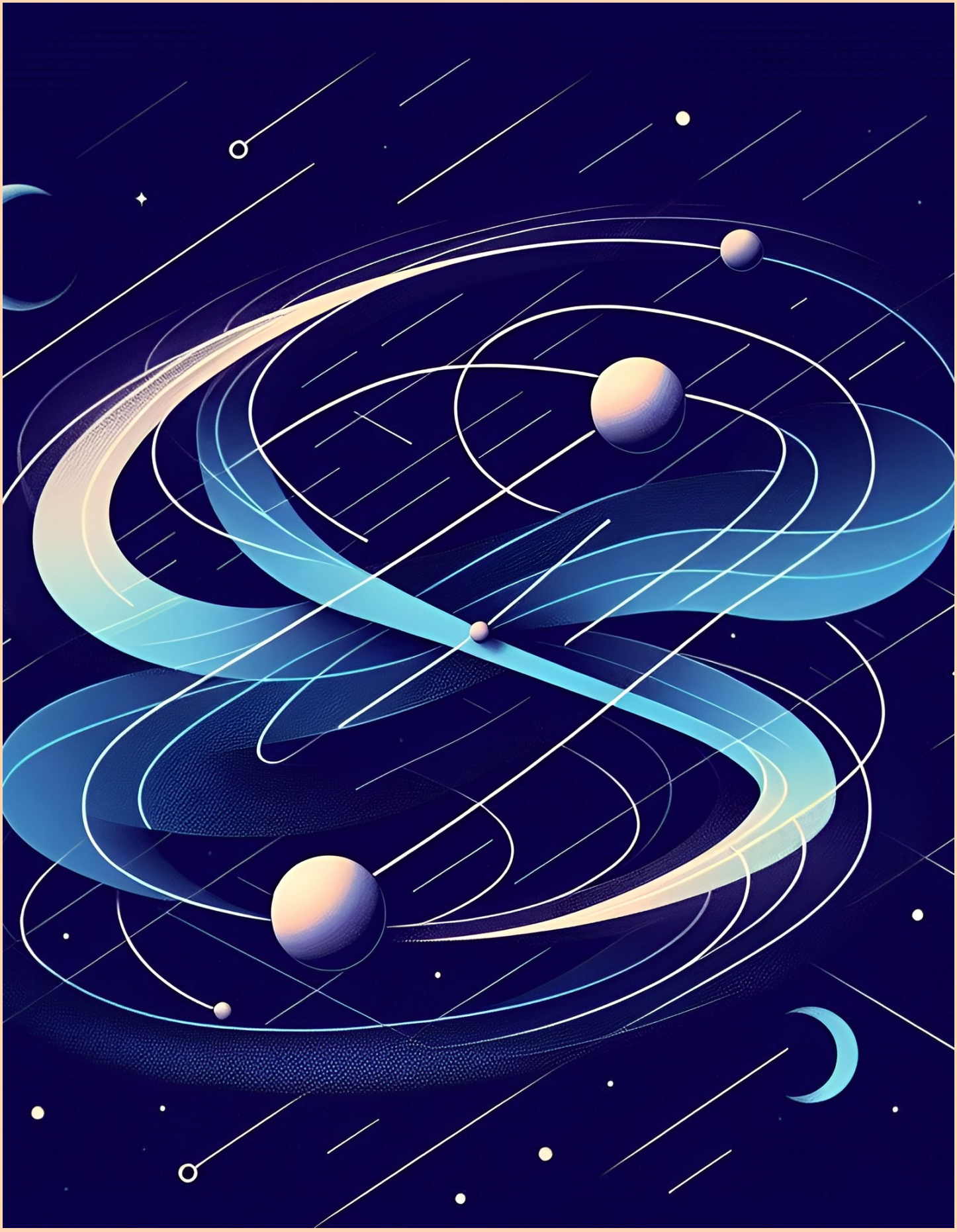

ISSN 3049-7930
February 2025

"If we knew what it was we were doing, it would not be called research, would it?"

Albert Einstein

Edinburgh Student Journal of Science
Volume 1
Issue 3
February 2025
ISSN 3049-7930

Published by the University of Edinburgh
Edited and Produced by Jack L Smith

Edinburgh Student Journal of Science

THE UNIVERSITY of EDINBURGH

journals.ed.ac.uk/esjs

Edinburgh Student Journal of Science

Volume 1, Issue 3, February 2025

Cover Illustration

The illustration on the journal cover of each issue is created based on one or more articles from within the issue which the editorial team found to be particularly well-written and engaging.

This issue features a more abstract cover to reflect the mathematical and theoretical focus of the articles within it. The image on this cover was created with the help of Microsoft Designer, however, in the future we hope to feature artwork from students; if you are interested in designing a future cover please email us!

Submitting to the Journal

We welcome submissions from later-year undergraduate, Master's, and recently graduated students within the College of Science and Engineering at the University of Edinburgh. Submissions should be no longer than 1500 words and should summarise work from academic/independent research projects, internships, or summer projects. Full details about submissions criteria and guidelines can be found on our website.

The Edinburgh Student Journal of Science is a student-run peer-reviewed journal for students studying science at the University of Edinburgh. It is an opportunity for students to publish formal summaries of their academic or independent research in a professional-style journal and get experience with the publishing and peer-review processes.

The journal is issued approximately every four months to coincide with the end of both academic semesters for academic projects, and the end of the summer break for summer projects or internships. We are continuously open for submissions, and a typical timeline of the submission process can be found online.

The next issue of the Edinburgh Student Journal of Science will be the first of our second volume, expected to be published in early July. For more information, templates, and guidance on submitting an article, please visit our website: journals.ed.ac.uk/esjs.

With all submissions to the journal being peer-reviewed by PhD students within the college, we are always looking for PhD students who wish to get involved reviewing. It is a rewarding experience and a great opportunity to develop and gain new skills; if you are interested in joining our team, please email us at ESJS@ed.ac.uk.

Contents

Physics and Astronomy

Physics and Astronomy

An Analysis of the Restricted Euler Problem Using Symplectic Integrators

Henry Yip*‡[1], Jennifer M. Smillie†[1]

[1] School of Physics and Astronomy, University of Edinburgh

Open Access

Received
29 Oct 2024

Revised
17 Nov 2024

Accepted
05 Jan 2025

Published
18 Feb 2025

Abstract

The Three-Body Problem is far from fully solved despite centuries of effort. The restricted Euler Problem is a special case in which two bodies are fixed in place, resulting in two Poisson-commuting conserved quantities, allowing the system to be fully integrable by the Liouville-Arnold theorem. We analysed the restricted Euler problem using an order-4 symplectic integrator, which conserves the Hamiltonian. We used this integrator to simulate the restricted Euler problem and recovered known orbits from the literature.

DOI: 10.2218/esjs.10064 **ISSN** 3049-7930

Introduction to the Restricted Euler Problem

Consider a two-dimensional system and consider the z-axis plotted against the x-axis. The two masses m_+ and m_- are located at $(0, b)$ and $(0, -b)$ respectively whereas the third mass can move around freely (Ó'Mathúna 2008). We then try to find the trajectory of the third particle based on Newton's gravitational law. As two of the masses are stationary, this problem is also called the problem of two fixed centers.

The problem is of interest because it is one of the restricted cases of the three-body problem in which the system is fully integrable, i.e. the system is fully analytic, allowing for prediction of orbits.

We first express the system in terms of planar prolate spheroidal coordinates:

$$x = \pm\sqrt{R^2 - b^2}\sin\sigma$$
$$z = R\cos\sigma$$

where $R \geq 0$, $\sigma \in [0, \pi]$. It is similar to the polar coordinate system but with two foci. Without loss of generality, we consider $b = 1$.

Expressing Prolate Spheroidal Coordinates using Cartesian Coordinates

In this section, we will express prolate spheroidal coordinates in terms of cartesian coordinates. Knowing the relation between both systems is useful as both are commonly used. We will focus on $x > 0$. When

*Student Author
‡Email: henry36c@gmail.com
†Corresponding academic contact: j.m.smillie@ed.ac.uk

$x < 0$, the values of R and σ correspond to those for $|x|$.

As $\cos\sigma$ is only negative in the range $\frac{\pi}{2} < \sigma < \pi$, we have $z > 0$ for $0 < \sigma < \frac{\pi}{2}$ and $z < 0$ for $\frac{\pi}{2} < \sigma < \pi$. Due to the nature of the solution, which will be apparent below, we will consider these two cases separately, and conclude by discussing $z = 0$.

Case for $z > 0$

Using $R = \frac{z}{\cos\sigma}$, we can substitute one of the equations into the other:

$$\begin{aligned} x &= \sin\sigma\sqrt{\left(\frac{z}{\cos\sigma}\right)^2 - 1} \\ &= \sqrt{\frac{z^2 - \cos^2\sigma}{\cos^2\sigma}}\sin\sigma \\ x^2 &= \frac{(z^2 - 1 + \sin^2\sigma)(\sin^2\sigma)}{1 - \sin^2\sigma} \\ x^2 &= \sin^2\sigma(x^2 + z^2 - 1 + \sin^2\sigma) \end{aligned}$$

where we have used $\cos\sigma = \sqrt{1 - \sin^2\sigma}$. This is only valid as $0 \leq \sigma \leq \frac{\pi}{2}$, which corresponds to $z > 0$. This is why we considered z separately.

By letting $u = \sin^2\sigma$, we have:

$$u^2 + (x^2 + z^2 - 1)u - x^2 = 0.$$

Using the quadratic formula, and noting that $\sqrt{u} = \sin\sigma$, we arrive at

$$\arcsin\sqrt{u} = \sigma_{z>0}$$

where

$$u = \frac{-(x^2 + z^2 - 1) + \sqrt{(x^2 + z^2 - 1)^2 + 4x^2}}{2}.$$

Case for $z < 0$

We have assumed $x > 0$ and found the solution for $z > 0$. We want to find the solution for $z < 0$ while keeping $x > 0$.

Note that $\sin(\pi - \sigma) = \sin\sigma$ and $\cos(\pi - \sigma) = -\cos\sigma$. As $x \propto \sin\sigma$ and $z \propto \cos\sigma$, by letting $\sigma_{z<0} = \pi - \sigma_{z>0}$, we can find solutions for $z < 0$.

Case for $z = 0$

We have:

$$\sigma = \begin{cases} \arcsin\sqrt{u} & \text{for } z > 0 \\ \pi - \arcsin\sqrt{u} & \text{for } z < 0 \end{cases}$$

where

$$u = \frac{-(x^2 + z^2 - 1) + \sqrt{(x^2 + z^2 - 1)^2 + 4x^2}}{2}.$$

By continuity, we have $\sigma = \frac{\pi}{2}$. Another way to think of it is that this coordinate system is the polar coordinate system being stretched in the oblate direction and mirrored at the z-axis. Therefore, similar to the polar coordinate system, when $z = 0$, the angle is $\frac{\pi}{2}$.

Listing the Conserved Quantities

The conserved quantities are important to both verify theoretical models and computational results and show the system is integrable.

It is important to note that both linear and angular momentum are not conserved, as two of the bodies are fixed in place, implying the existence of external forces. This can be illustrated by releasing the third body a distance away from the two fixed bodies. The initial linear and angular momentum are zero, but the third body is attracted by the two fixed bodies and accelerates towards them.

We define two constants, g and h, below (Dullin *et al.* 2016):

$$g = \frac{1}{2}\left(zp_x - xp_z\right)^2 + \frac{1}{2}b^2p_z^2 + bz\left(\frac{m_1}{\sqrt{(z+b)^2+x^2}} - \frac{m_2}{\sqrt{(z-b)^2+x^2}}\right)$$
$$h = \frac{1}{2}\left(p_z^2 + p_x^2\right) - \frac{m_1}{\sqrt{(z+b)^2+x^2}} - \frac{m_2}{\sqrt{(z-b)^2+x^2}}$$

where b, as defined above, is the distance of the two centers from the origin, and p_x and p_z are momentum in the x and z directions, respectively. We take $b = 1$, and therefore:

$$g = \frac{1}{2}\left(zp_x - xp_z\right)^2 + \frac{1}{2}p_z^2 + bz\left(\frac{m_1}{\sqrt{(z+1)^2+x^2}} - \frac{m_2}{\sqrt{(z-1)^2+x^2}}\right)$$
$$h = \frac{1}{2}\left(p_z^2 + p_x^2\right) - \frac{m_1}{\sqrt{(z+1)^2+x^2}} - \frac{m_2}{\sqrt{(z-1)^2+x^2}}$$

where g is a symmetry in the phase space, and h is the energy of the third particle. It can also be shown that g is a first integral of motion and the two constants commute under the Poisson bracket. Hence, the system is integrable by the Liouville-Arnold theorem.

Choosing an Integration Method for Numerical Simulation

Below, we aim to choose an integration method that can be used for a general three-body problem, so we assume all three bodies can move freely. As we are integrating a Liouville integrable system, we choose symplectic integrators, which conserve the Hamiltonian. This is discussed extensively in Casey (2020), which we will use for the whole section.

Starting from $i = 1$, we denote each particle by m (m ranges from 1-3). Using x and v to represent positions and velocities, respectively, we first run:

$$v_m^{(i)} = v_m^{(i-1)} + c_i a(x_m^{(i-1)})dt$$

for each m, in order of $m = 1$, $m = 2$, then $m = 3$. c_i is an integer, which is further explained below. dt is the step size in the numerical simulation. After this step, we run:

$$x_m^{(i)} = x_m^{(i-1)} + d_i v_m^{(i)} dt$$

for each m, as above. We have d_i as an integer. After these two steps are run, we increase i by 1. This process repeats until i reaches n, where n is defined as the order of the symplectic integrator. The whole process is illustrated in the example below, corresponding to $n = 2$:

Particle 1, Steps 1-6

$$
\begin{aligned}
v_1^{(1)} &= v^{(0)} + c_1 a(x^{(0)})dt \\
x_1^{(1)} &= x^{(0)} + d_1 v^{(1)} dt \\
v_2^{(1)} &= v^{(0)} + c_1 a(x^{(0)})dt \\
x_2^{(1)} &= x^{(0)} + d_1 v^{(1)} dt \\
v_3^{(1)} &= v^{(0)} + c_1 a(x^{(0)})dt \\
x_3^{(1)} &= x^{(0)} + d_1 v^{(1)} dt
\end{aligned}
$$

Particle 2, Steps 7-12

$$
\begin{aligned}
v_1^{(2)} &= v^{(1)} + c_2 a(x^{(1)})dt \\
x_1^{(2)} &= x^{(1)} + d_2 v^{(2)} dt \\
v_2^{(2)} &= v^{(1)} + c_2 a(x^{(1)})dt \\
x_2^{(2)} &= x^{(1)} + d_2 v^{(2)} dt \\
v_3^{(2)} &= v^{(1)} + c_2 a(x^{(1)})dt \\
x_3^{(2)} &= x^{(1)} + d_2 v^{(2)} dt
\end{aligned}
$$

For compactness, we can put all the c_i and d_i into a vector:

$$
\begin{aligned}
\mathbf{c} &= [c_1, c_2, ..., c_{n-1}, c_n] \\
\mathbf{d} &= [d_1, d_2, ..., d_{n-1}, d_n].
\end{aligned}
$$

Furthermore, we can put $\mathbf{c}$ and $\mathbf{d}$ into a matrix:

$$
\mathbf{A} = \begin{pmatrix} \mathbf{c} \\ \mathbf{d} \end{pmatrix}.
$$

Types of Symplectic Integrators

It has been shown by Casey (2020), firstly, that

$$
\mathbf{A} = \begin{pmatrix} 1 \\ 1 \end{pmatrix}
$$

leads to a first-order symplectic integration method; this is the Euler method. Meanwhile,

$$
\mathbf{A} = \begin{pmatrix} \frac{1}{2} & \frac{1}{2} \\ 1 & 0 \end{pmatrix}
$$

leads to a second-order symplectic integration method; the Verlet method. Furthermore,

$$
\mathbf{A} = \begin{bmatrix} \frac{7}{24} & \frac{3}{4} & \frac{-1}{24} \\ \frac{2}{3} & \frac{-2}{3} & 1 \end{bmatrix}
$$

leads to a third-order symplectic integration method, referred to as the Ruth method. And lastly,

$$
\mathbf{A} = \begin{bmatrix} \frac{1}{2\left(2-2^{1/3}\right)} & \frac{1-2^{1/3}}{2\left(2-2^{1/3}\right)} & \frac{1-2^{1/3}}{2\left(2-2^{1/3}\right)} & \frac{1}{2\left(2-2^{1/3}\right)} \\ \frac{1}{2-2^{1/3}} & \frac{-2^{1/3}}{2-2^{1/3}} & \frac{1}{2-2^{1/3}} & 0 \end{bmatrix}
$$

leads to a fourth-order symplectic integration method, which will be referred to as the Neri method. In theory, a n^{th} order symplectic method is supposed to have an error of $O(h^n)$, where h is the step size of the system. Therefore, the error should drop as the order of the method increases.

Metrics for Choosing an Integration Method

We used several metrics to evaluate the precision of the numerical methods specified above. As we built this code with the purpose of simulating the general three-body problem, these metrics were compared across three different orbits, namely the Figure-8 orbit, the Bumblebee orbit, and the Moth orbit. Each orbit was simulated with a total of $100,000$ steps, using a step size of 0.0001.

The first metric compares the error of energy to the initial energy, which can be named as energy deviation:

$$
\frac{\Delta E}{E_0} = \left| \frac{E_{\text{max}} - E_{\text{min}}}{E_0} \right|
$$

where E_0 is the energy at the start of the simulation.

The second metric is named the momentum difference. For many systems, the initial momentum is zero. Therefore, a momentum deviation cannot be well defined. Instead, we will only check the momentum difference, which can be defined as:

$$\text{Max } \Delta p_x = |p_{\max,x} - p_{\min,x}|$$
$$\text{Max } \Delta p_y = |p_{\max,y} - p_{\min,y}|.$$

The third metric is the run time. In our scenario, most simulations are relatively short, so it is not as important as the metrics above. Below all the metrics are compared for each orbit.

Method	Orbit	Energy Deviation	Max Δp_x	Max Δp_y	Run Time (s)
Neri (Order 4)	Figure-8	6.124×10^{-14}	1.040×10^{-13}	4.852×10^{-14}	29.60
Ruth (Order 3)	Figure-8	1.280×10^{-13}	5.307×10^{-14}	3.048×10^{-14}	25.91
Verlet (Order 2)	Figure-8	5.893×10^{-9}	3.841×10^{-14}	2.232×10^{-14}	12.31
Euler (Order 1)	Figure-8	3.601×10^{-5}	3.686×10^{-14}	3.009×10^{-14}	15.53
Neri (Order 4)	Bumblebee	8.058×10^{-3}	4.591×10^{-14}	9.246×10^{-14}	27.79
Ruth (Order 3)	Bumblebee	8.058×10^{-3}	7.394×10^{-14}	4.249×10^{-14}	23.84
Verlet (Order 2)	Bumblebee	9.676×10^{-2}	2.287×10^{-14}	1.882×10^{-14}	11.56
Euler (Order 1)	Bumblebee	2.4329	3.625×10^{-14}	2.312×10^{-14}	15.71
Neri (Order 4)	Moth	1.459×10^{-9}	4.874×10^{-14}	8.693×10^{-14}	28.06
Ruth (Order 3)	Moth	2.143×10^{-8}	3.486×10^{-14}	3.185×10^{-14}	22.39
Verlet (Order 2)	Moth	4.775×10^{-5}	2.387×10^{-14}	3.835×10^{-14}	11.55
Euler (Order 1)	Moth	0.02070	2.031×10^{-14}	2.183×10^{-14}	13.76

Table 1: Comparison of Ruth, Neri, Verlet, and Euler methods across different orbits.

First, the Euler method has the highest energy inaccuracy by far, while having a higher running time than the Verlet method. The latter result is surprising, and is possibly due to the 0 entry in the d_2 corresponding to the Verlet method. Besides, it can be seen that the Neri method conserves energy much better than other methods, especially in the Moth orbit simulation. More interestingly, the Verlet method conserves momentum slightly better than methods with higher orders. However, the difference is too small to be significant (all of order 10^{-14}), and may not be accurate, as they are close to the machine error for double-precision floating-point numbers in Python, which is $O(10^{-16})$. Even though the Neri method causes a longer run time, the difference is negligible. Therefore, the Neri method is chosen.

Results

Types of Orbits

We have reproduced three types of orbits as described in Dullin *et al.* (2016). First, we reproduced the satellite orbit, in which the z-coordinate of the third body never changes sign. In other words, the third body never seems to pass through the mid-point between the two fixed centers. Next, we reproduced the planetary orbit, in which the third body almost forms a complete ellipse around the two centers. Finally, we reproduced the lemniscate orbit, in which the third body passes through the line connecting the two fixed centers, unlike both satellite and planetary orbits. The trajectories of the orbits are included in the GitHub repository available at the end of this paper.

Predicting Type of Orbit from Integrals of Motion

Referring to g and h, as defined above, the value of h must be negative, as we are solving a bounded system, but the values for g greatly vary. It has been shown in literature (Dullin *et al.* 2016) that g and h, the integrals of motion shown above, can predict the type of orbit. In general, negative g corresponds to a satellite orbit, a slightly positive g (say, between 0 and 1) corresponds to a lemniscate orbit, and a larger g corresponds to a planetary orbit. This is different for different combinations of m_+ and m_-, but we only considered the symmetric case. We have verified that the satellite orbit corresponds to $g < 0$ and $h < 0$, the lemniscate orbit corresponds to $0 < g < 1$ and $-1 < h < 0$, and the planetary orbit corresponds to $g > 1$ and $-0.5 < h < 0$, which agrees with literature (Dullin *et al.* 2016).

Textbook Verification by Comparing Eccentricities and Semi-major Axes

To conclude, we can compare with the constants defined by Ó'Mathúna (2008). It is defined that M and N are constants, where

$$\frac{1}{2}\frac{\left(R^2 - b^2\cos^2\sigma\right)^2}{R^2 - b^2}\dot{R}^2 = ER^2 + \mu R + M$$
$$\frac{1}{2}\left(R^2 - b^2\cos^2\sigma\right)^2\dot{\sigma}^2 = -Eb^2\cos^2\sigma + \frac{(m_+ - m_-)\mu b\cos\sigma}{m_+ + m_-} + N.$$

We have $\mu = G(m_1 + m_2)$ and G is the gravitational constant between particles, which is usually taken as 1 for simplicity.

It is stated in the textbook that when $\eta^2 < 1$, it corresponds to a closed elliptic orbit of eccentricity η and semimajor axis p. The two constants are defined as:

$$p = \frac{O^2}{2}$$
$$\eta = \frac{1}{p}$$

where $O = \sqrt{2N}$ is a constant with units of angular momentum. In our code, only the planetary orbit satisfies $\eta^2 < 1$. This agrees with theoretical results, as the planetary orbit is the only type of closed orbit.

To verify our estimate of the semi-major axis p is accurate, we have also measured the semi-major axis of a planetary orbit directly from its trajectories in the x-z plane. If the code is accurate, using $\eta = \frac{1}{p}$, we should obtain $p = 2.35$ if we use an orbit with $\eta = 0.425$. Instead, we obtained $p = 2.53$ with a standard deviation of 0.133, showing a small discrepancy. This inaccuracy should be investigated over a range of η values.

Conclusion

We selected an integration method and used it to analyze Euler's Three Body Problem. We demonstrated that the three types of orbits in the Euler Problem can be recreated. Further work could involve simulating and exploring different cases discussed by Ó'Mathúna (2008), as well as comparing results with other integrator types, such as regularized integrators and adaptive step size integrators.

Data Availability

The code used in this project, as well as some additional diagrams are available on GitHub: `https://github.com/Henry-Yip/Three_Body_Problem_Code`.

Acknowledgements

I would like to express my gratitude to Prof. Jenni Smillie for generously taking the time to supervise this project. I am also thankful to the School of Physics and Astronomy, University of Edinburgh for funding this project through the Career Development Scholarship. Additionally, I would like to thank Allison Lau (University of Toronto) for her encouraging comments.

References

Casey, R. M. 'Computer Implementation of Symplectic Integrators and Their Applications to the N-body Problem' (2020)

Dullin, H. R. and Montgomery, R. 'Syzygies in the Two Center Problem' Nonlinearity **29** 4 (2016)

Ó'Mathúna, D. 'Integrable Systems in Celestial Mechanics' (Springer Science & Business Media; 2008)

Parameterized Post-Friedmann Formalism for the Dark Scattering Model

Durrah Alessa*[1], Pedro Carrilho†[1]

[1] School of Physics and Astronomy, University of Edinburgh

Open Access

Received
31 Oct 2024

Revised
17 Dec 2024

Accepted
08 Jan 2025

Published
18 Feb 2025

Abstract

Recent results from the Dark Energy Spectroscopic Instrument find a preference for dynamical dark energy. This motivates improving the accuracy of predictions for dynamical dark energy models, including those which can resolve current tensions in the data, such as the dark scattering model. We improve the parameterized post-Friedmann approach for this model, reducing the error from approximately 1.3% to only 0.1%. Additionally, we show that the commonly used scale-independent approximation may not be completely accurate and, when applying the best-fit values from DESI on the dark scattering model, we predict an enhancement of the power spectrum at late times, worsening the S_8 tension.

DOI: 10.2218/esjs.10094 **ISSN** 3049-7930

Introduction

On large scales, our universe consists of three main components: baryons, dark matter, and dark energy. Dark energy, which represents $\simeq 70\%$ of the universe, is responsible for accelerating the universe's expansion. While we understand the impact of dark energy on the universe, its fundamental nature remains unknown. However, several explanations for dark energy have been proposed such as the dynamical dark energy w_0w_aCDM (Chevallier *et al.* 2001), modified gravity (Tsujikawa 2010), and interacting dark energy models (van der Westhuizen *et al.* 2024).

The widely accepted standard cosmological model, ΛCDM, struggles to explain recent data discrepancies in cosmology such as the S_8 tension, which refers to a difference between the direct measurements of the clustering of matter in the late universe and the value inferred from the Cosmic Microwave Background (CMB) probing the early universe (Perivolaropoulos *et al.* 2022). As a result, several models beyond the ΛCDM model have appeared, including the Dark Scattering model (Simpson 2010), which introduces a scattering between the dark matter particles and the dark energy fluid similar to the Thompson scattering between electrons and photons. With the appropriate interaction strength, this model provides a promising explanation for the lower value of the S_8 parameter at late times.

Furthermore, the latest results from the Dark Energy Spectroscopic Instrument (DESI) indicate that the equation of state parameter of dark energy w – defined as its energy density divided by its pressure – crosses the phantom divide, corresponding to a value of $w = -1$ (DESI Collaboration *et al.* 2024). This motivates improving the accuracy of predictions of dark energy models that cross $w = -1$, and the Parameterized Post-Friedmann (PPF) approximation is the most general way to do that, which applies to most models of dynamical dark energy (Fang *et al.* 2008). This paper aims to enhance the accuracy of the PPF approximation for the dark scattering model to ensure that it can be confidently tested with the most precise data, minimizing potential biases.

PPF Formalism for the Dark Scattering Model

The PPF formalism offers a way of studying extensions to the standard cosmological model. It achieves this by introducing parameters that quantify those deviations within a well-defined formalism (Baker

*Student Author
†Corresponding academic contact: pedro.carrilho@ed.ac.uk

et al. 2013). In the context of dark energy, the PPF formalism has been tested in cases where the fluid approximation works well and then applied to cases where it breaks down, specifically those involving the crossing of the phantom divide $w = -1$.

In the fluid approximation, dark energy is treated as a fluid, allowing the application of hydrodynamic equations to describe its behaviour (Lesgourgues 2013). In the dark scattering case, the Euler equations for both dark energy and dark matter are modified by a drag term $a\xi_{ds}\rho_c\Delta\theta$, due to the scattering of the dark matter particles of the dark energy fluid (Simpson 2010), where

$$\xi_{ds} = \frac{\sigma_D}{m_c} \tag{1}$$

is the dark scattering parameter. The two Euler equations represent the evolution equations for the velocity perturbations for both dark energy e and dark matter c.

$$\theta'_e = 2\mathcal{H}\theta_e + k^2\Psi + k^2\frac{\delta_e}{1+w} - a\xi_{ds}\rho_c\Delta\theta \tag{2}$$

$$\theta'_c = -\mathcal{H}\theta_c + k^2\Psi + (1+w)a\xi_{ds}\rho_e\Delta\theta \tag{3}$$

The prime in the above equations denotes the derivative with respect to conformal time, $\frac{d}{d\eta}$. Here, a is the scale factor, and

$$\mathcal{H} = \frac{a'}{a} \tag{4}$$

is the Hubble parameter. In the second term, k is the wave number, and Ψ denotes the perturbation to the Newtonian potential. In the third term, δ_e represents the perturbation of the dark energy density. In the last term $\Delta\theta$ is the difference between the velocity perturbation of dark energy and dark matter, defined as $\Delta\theta = \theta_e - \theta_c$, where $\theta_e = \nabla \cdot V_e$ and $\theta_c = \nabla \cdot V_c$. In equation 2, the third term is undefined in the case of $w = -1$, which indicates the need for the PPF formalism. The construction of the PPF formalism replaces the fluid equations of dark energy with an alternative set describing the evolution of its fluctuations over the phantom divide. We follow the PPF approach as discussed in both Fang *et al.* (2008) and Li *et al.* (2014), and extend it to the dark scattering case.

Generally, in the PPF approach, a dynamical parameter Γ is introduced at large scales that reduces to the Poisson equation at small scales, where dark energy is assumed to be smoothed:

$$\Phi + \Gamma = \frac{4\pi G}{k_H^2 H^2}\Delta_T\rho_T \tag{5}$$

Here, Φ represents the perturbation to the spatial curvature and is related to Ψ in Equations 2 and 3 by $\Phi = -\Psi$ in the absence of anisotropic stress. This equation, excluding Γ, represents one of Einstein's equations in Newtonian gauge, as detailed in Hu *et al.* (1999) and Fang *et al.* (2008). On the right-hand side, $k_H = \frac{k}{aH}$ is the modified wave number, G is the gravitational constant, ρ_T is the total matter energy density, Δ_T is the density perturbation of matter – excluding dark energy – in the total matter gauge.

The equation of motion for equation 5, at all scales, is expressed as

$$(1 + c_\Gamma^2 k_H^2)[\Gamma' + \Gamma + c_\Gamma^2 k_H^2 \Gamma] = S \tag{6}$$

The introduction of c_Γ terms above imposes the physical condition that dark energy fluctuations vanish on sufficiently small scales ($k_H \gg 1$) as a consequence of having a sound speed close to that of light in most models of dark energy (which is also assumed here). As before, the prime denotes differentiation with respect to $\ln a$. The source term is represented by S.

In the case of generic interacting models, energy and momentum exchange contribute to the source term, S. However, only momentum exchange is considered for dark scattering, the contribution of which is denoted by f_c, as defined in Li *et al.* 2014. To find the correct expression of f_c in the case of dark scattering, we use the modified Euler equations (Eqs. 2 and 3), and find

$$f_c = \frac{\xi_{ds}}{k}\rho_c\Delta\theta(\rho_e + p_e) \tag{7}$$

We consider this expression when we derive the source term for the dark energy perturbations, S, and the resulting source term becomes

$$S = \left[\frac{4\pi G}{k_H^2 H^2}(\rho_e + p_e)\left(k_H V_T + \frac{3Z}{k_H}(V_T - V_c)\right) - \frac{3aZ}{F}c_\Gamma^2\Gamma\right]\left[1 + \frac{3ZC}{k_H^2 F}\right]^{-1} \tag{8}$$

with

$$Z = \frac{\xi_{ds}\rho_c}{H}, \qquad C = 1 - \frac{1}{1 + c_\Gamma^2 k_H^2}, \qquad F = 1 + 3\frac{4\pi G}{k_H^2 H^2}(\rho_T + p_T) \tag{9}$$

Here, ρ_c and ρ_e are the dark matter and dark energy density, respectively. Both p_e and p_T are the dark energy and total matter pressure, respectively. The total matter velocity is represented by V_T. This result comes from deriving equation 5 and using both Equations 2 and 3. This formula represents our first main result, which enables us to improve the accuracy of predictions relative to the standard PPF formula (with $Z = 0$), demonstrated below.

Results

We implemented the new modified source term in the Cosmic Linear Anisotropy Solving System (CLASS) (Blas *et al.* 2011). We obtained an improved accuracy of predictions for the expected matter power spectrum ratio $P/P_{\Lambda CDM}$ from approximately 1.3% to 0.3% difference overall between the fluid result and the PPF result. A value of $c_\Gamma = 0.4$ is typically used for standard dark energy models, but this requires validation in the dark scattering case. We tested different c_Γ and found a value of $c_\Gamma = 0.15$ maximizes the accuracy of predictions, to approximately 0.1% difference overall. Fig 1a shows the resulting power spectrum ratio plotted against the scale, k, before and after modifying the source term in the PPF approximation, compared to the fluid approximation in a case with constant w. This improved accuracy allowed us to test different scenarios of the dark scattering model crossing the phantom divide, where we consider the Chevallier-Polarski-Linder (CPL) parameterization for the equation of state

$$w(a) = w_0 + w_a(1 - a) \tag{10}$$

as in Chevallier *et al.* (2001) and Linder (2003).

We show an interesting case in Figure 1b, where the power spectrum ratio is plotted before and after correction for the case of $w_0 = -1.15$ and $w_a = 0.5$. The difference between the two is notable, demonstrating the improved accuracy our predictions following the above modifications. Figure 1b also indicates that the commonly used scale-independent approximation for the power spectrum in the range of $10^{-2} < k < 10^{1}$ may not be accurate in some cases. This approximation is generally valid on small scales (i.e., large values of k) because the dark matter equation does not depend on the scale and dark energy fluctuations are considered negligible. With the help of the scale-independent approximation presented in Carrilho *et al.* (2022) for the dark scattering case, we show the difference between the scale-independent approximation and the full calculation labelled "After" in Figure 1b. The difference between the two indicates the need to use the modified source term in analysing real data when considering dark scattering.

Applying the best-fit values for w_0 and w_a from DESI Collaboration *et al.* (2024), we find that the dark scattering model does not suppress the power spectrum, but rather enhances it at late times. Figure 1c shows the resulting power spectrum ratio from the best-fit values from the three SN Ia data sets. This result indicates that, if the universe is described by these values of w_0 and w_a, then the dark scattering model is not a solution for the S_8 tension, which requires instead a suppression at late times.

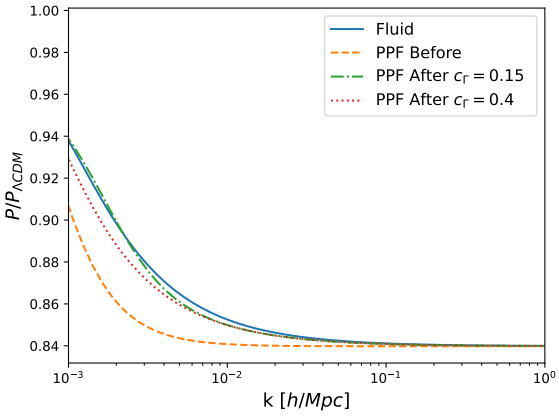

(a)

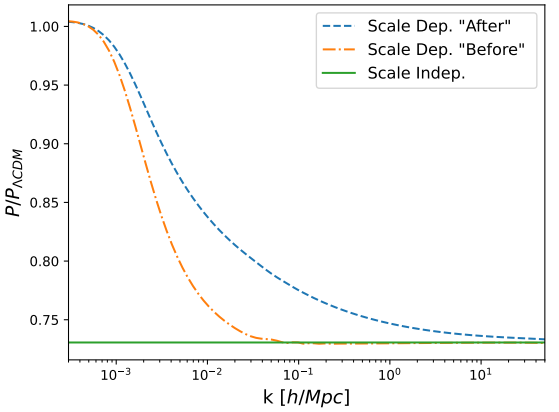

(b)

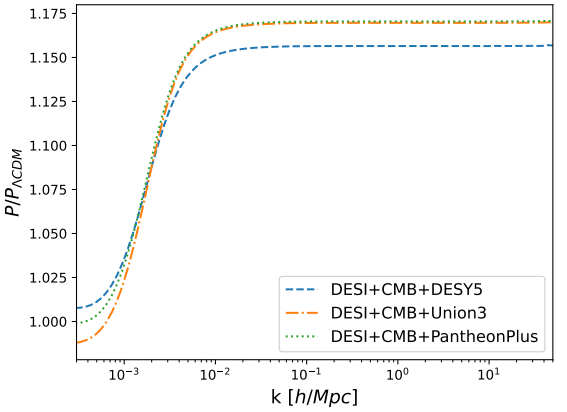

(c)

Figure 1: The power spectrum ratio $P/P_{\Lambda CDM}$ is plotted against the scale k at $z = 0$ using a value of $\xi_{ds} = 50\text{b/GeV}$. (a) The PPF approximation before and after modifying the source term is compared with the fluid approximation for the dark scattering case $w = -0.9$. (b) The plot shows the crossing of the $w = -1$ case with the following values $w_0 = -1.15$ and $w_a = 0.5$ before and after modifying the source term, compared with the scale-independent approximation. (c) The three DESI cases correspond to the central values from the three SN Ia data sets: $w_0 = -0.727$ and $w_a = -1.05$, $w_0 = -0.64$ and $w_a = -1.27$, $w_0 = -0.827$ and $w_a = -0.75$.

Conclusions

In this paper, we improve the accuracy of the PPF formalism for the dark scattering model, enabling confident testing of phantom crossing cases for this model. A notable result revealed by our predictions following modifications, is the substantial scale dependence of the power spectrum ratio within the scale range $10^{-2} < k < 10^{1}$ in some cases, requiring careful analysis of real data within this scale range. We also make predictions for the values of w_0 and w_a favoured by DESI, finding that if they accurately represent the real universe, the dark scattering model cannot resolve the S_8 tension, as it would instead enhance clustering. A detailed exploration of this model with the DESI data is therefore needed in the future.

Acknowledgments

I am deeply grateful to my supervisor, Dr. Pedro Carrilho, for his insightful guidance, patience, and encouragement throughout this research project. I would also like to thank Prof. Florian Beutler for his helpful advice and contributions. This research was funded as a part of the Custodian of the Two Holy Mosques scholarship program. Finally, my deepest thanks go to my sisters for their unwavering support.

References

Baker, T. *et al.* 'The Parameterized Post-Friedmann Framework for Theories of Modified Gravity: Concepts, Formalism, and Examples' Physical Review D **87** 2 (2013)

Blas, D. *et al.* 'The Cosmic Linear Anisotropy Solving System (CLASS). Part II: Approximation Schemes' Journal of Cosmology and Astroparticle Physics **2011** 07 (2011)

Carrilho, P. *et al.* 'On the Road to per Cent Accuracy VI: The Non-linear Power Spectrum for Interacting Dark Energy With Baryonic Feedback and Massive Neutrinos' Monthly Notices of the Royal Astronomical Society **512** 3 (2022)

Chevallier, M. and Polarski, D. 'Accelerating Universes With Scaling Dark Matter' International Journal of Modern Physics D **10** 02 (2001)

DESI Collaboration *et al.* 'DESI 2024 VI: Cosmological Constraints From the Measurements of Baryon Acoustic Oscillations' arXiv e-prints (2024)

Fang, W. *et al.* 'Crossing the Phantom Divide With Parametrized Post-Friedmann Dark Energy' Physical Review D **78** 8 (2008)

Hu, W. and Eisenstein, D. J. 'Structure of Structure Formation Theories' Physical Review D **59** 8 (1999)

Lesgourgues, J. 'TASI Lectures on Cosmological Perturbations' arXiv e-prints (2013)

Li, Y.-H. *et al.* 'Parametrized Post-Friedmann Framework for Interacting Dark Energy' Physical Review D **90** 6 (2014)

Linder, E. V. 'Exploring the Expansion History of the Universe' Physical Review Letters **90** 9 (2003)

Perivolaropoulos, L. and Skara, F. 'Challenges for ΛCDM: An Update' New Astronomy Reviews **95** (2022)

Simpson, F. 'Scattering of Dark Matter and Dark Energy' Physical Review D **82** 8 (2010)

Tsujikawa, S. 'Modified Gravity Models of Dark Energy' in Lectures on Cosmology (Springer Berlin Heidelberg; 2010)

Van der Westhuizen, M. A. and Abebe, A. 'Interacting Dark Energy: Clarifying the Cosmological Implications and Viability Conditions' Journal of Cosmology and Astroparticle Physics **2024** 01 (2024)

Journal Acknowledgements

Thanks again to all who have helped and been involved with the production of the this issue, and the first volume as a whole, particularly members of the editorial board for their continuous advice to improve the journal. Additional thanks to the College of Science and Engineering Engagement Team (Marianne, Kenny and Chris) for their help in publicising the journal to a much broader audience, as well as to Linda Kirstein for her assistance with this.

As always, an additional thank you to Edinburgh Diamond and their team who enable the publication of the journal, as well as to the team of over 20 PhD students who give their time to serve as reviewers, even though their expertise was not required for this particular issue.

Jack L Smith, Editor-in-Chief